Effect of Textures on Tensile Properties of Extruded Ti64/VGCF Composite by Powder Metallurgy Route

Patchara Pripanapong, Shu-Feng Li, Junko Umeda, Katsuyoshi Kondoh

Effect of Textures on Tensile Properties of Extruded Ti64/VGCF Composite by Powder Metallurgy Route

Patchara Pripanapong[1], Shu-feng Li[2], Junko Umeda[2], Katsuyoshi Kondoh[2]

1 – Graduated School of Engineering, Osaka University, 2-1, Yamadaoka, Suita, Osaka, Japan

2 – Joining and Welding Research Institute, Osaka University, 11-1 Mihogaoka, Ibaraki, Osaka, Japan

DOI **10.13140/RG.2.1.1120.1525**

Keywords: Ti-6Al-4V, VGCFs, composite materials, hot extrusion, dynamic recrystallization.

ABSTRACT. Monolithic Ti-6Al-4V and Ti-6Al-4V composited with vapor grown carbon fibers (VGCFs) were fabricated by powder metallurgy (P/M) route in this research. Spark plasma sintering (SPS) subsequent by hot extrusion was applied in order to fabricate a full-density and high strength composite materials. A severe plastic deformation during hot extrusion resulted in a dynamic recrystallization (DRX) in α-Ti grains. Dynamic recrystallization was observed in a low deformation temperature region, which yield point of material was also observed in the stress-strain curve. Furthermore, the addition of VGCFs encouraged the dynamic recrystallization during hot extrusion. Ti64+0.4 wt-% VGCFs shows the highest tensile strength of 1192 MPa at the end part of the extruded rod where the temperature of material was lower compared to the tip and middle part during extrusion. Additionally, the improvement in tensile strength was contributed by solid-solution strengthening of carbon element originated from VGCFs in α-Ti matrix.

Introduction. Ti-6Al-4V alloy (Ti64) is the most well-known among Ti alloys, and used in many industries. High specific strength, good corrosion resistance and biocompatibility promoted a widely use of Ti and its alloys such as in aerospace and automobile industries, or medical devices and prosthesis [1, 2]. Many researchers studied the effect of hot working on microstructure and mechanical properties of wrought or cast Ti64. A. Momeni et al. studied the effect of deformation temperature and strain rate on microstructure and flow stress of wrought Ti64 under hot compression test [3]. Ti64 specimens, which experienced a hot compression test at 1273 and 1323 K, exhibited a large recrystallized α-grain with low flow stress on the microstructure. This correlated with the results proposed by T. Seshacharyulu et al. and R. Ding et al. for the cast Ti64 [4, 5]. G.Z. Quan et al. studied the modelling for dynamic recrystallization in Ti-6Al-4Al by hot compression test. The result shows that a flow stress decreases with the increasing of deformation temperature. The high deformation temperature promotes the mobility at the boundaries for annihilation of dislocation, and the nucleation and growth of dynamic recrystallization [6]. H.Z. Niu et al. studied the phase transformation and dynamic recrystallization (DRX) behaviour of Ti-45Al-4Nb-2Mo-B (at-%) alloy. The results show that the DRX modes were strongly depends on deformation temperature, and a decomposition of lamellar structure along with the DRX of γ and B2/β grain occurred at low forging temperature [7]. D.L. Ouyang et al. studied the recrystallization behaviour of Ti-10V-2Fe-3Al alloy after hot compression test. They reported that a partial grain refinement related to incomplete DRX was observed even after a large strain of 1.6, and an increment of strain resulted in an increasing of volume fraction of recrystallized grain. The full grain refinement accompanied by the completely DRX was developed at lower temperature of 1223 K by severe deformation [8]. The dynamic recrystallization behaviour of Ti-5Al-5Mo-5V-1Cr-1Fe alloy was reported by H. Liang et al. The DRX always occur when the store energy in a material reaching the critical value. During hot deformation, the increase of flow stress caused by dislocation generation and interaction resulted in an improvement of strength of Ti alloys. The sample deformed at 1073 K exhibited higher tensile strength compared to sample deformed at 1153 K because more dislocations were generated [9]. There are many reports related to dynamic

recrystallization of Ti alloys but no report in dynamic recrystallization behaviour of Ti64 composite with VGCF, and its effect on tensile properties of composite material was found yet [10, 12]. The objective of this research is to study the texture of Ti64 and Ti64 composites fabricated by spark plasma sintering, and subsequently hot extruded. The effect of dynamic recrystallization on tensile properties of monolithic Ti64 and Ti64/VGCF composite materials were investigated through this research. The samples cut from the end and middle part of extruded rod (extruded temperature lower than 1243 K) show a DRX structure which many of small nucleated grains were observed. Tensile sample obtained from the part that experienced extrusion at low temperature exhibited a high tensile strength because a large amount of defects was generated in a sample.

Experimental procedure. Ti-6Al-4V atomization powder (Osaka Titanium Technology Co., Ltd. TILOP64-45) with a spherical shape and diameter of 45 μm (fig. 1a), and vapor grown carbon fibers (Showa Denko K.K.,VGCFs^{TM}) with 8 μm in length and diameter of 150 nm (fig. 1b) were applied in this research. The chemical composition of Ti64 powder was listed in Table 1. Ti64 powder was mixed with cleasafe oil (0.15 g) by table milling equipment for 3.6 ks with rotation speed of 90 rpm and subsequently mixed with VGCFs by rocking milling for 7.2 ks. Rocking milling was performed for long time in order to provide a uniform distribution of VGCFs on powder surface. The Ti64 composite materials were fabricated in three compositions such as 0, 0.1 and 0.4 wt-% of VGCFs. The Ti64/VGCFs mixed powder was poured in the carbon container, which has an inner diameter of 42 mm. The inner wall of container was sprayed with boron nitride to prevent a reaction between Ti64 powder and carbon container during SPS. The monolithic Ti64 and mixed Ti64/VGCFs powder were pre-compacted by hydraulic hand press under pressure of 20 MPa before sintering. The green compacts were consolidated by spark plasma sintering (Syntech CO. SPS103S) at 1273 K with heating rate of 0.54 K/s for 1.8 ks, and the pressure of 30 MPa was introduced to a green compact under vacuum atmosphere of 5 Pa. Afterwards, the sintered billets were preheated in a horizontal image furnace at 1323 K for 0.6 ks under argon atmosphere before hot extruded into 12 mm in diameter rod by 200 ton press machine (THK Slidepack FBW3950R 1200L) with an extrusion speed of 6 mm/s. The sintered billets and extruded specimens were cut for microstructure observation. For extruded rod, the samples were cut from three positions which are shown in fig. 2. The samples were ground with SiC abrasive paper, polished with Al_2O_3 colloidal and etched by Kroll etchant (H_2O:HNO_3:HF = 100:5:1) for microstructure observation. For EBSD analysis, the specimens were polished with SiO_2 colloidal by vibratory polisher. The microstructures observation and phase analysis of sintered and extruded specimens were performed by optical microscope and scanning electron microscope (JEOL JSM6500F). The grain size and texture were analysed by electron back-scatter diffraction (EBSD) method. The tensile samples were machined from three positions in extruded rod (fig. 2) with 20 mm in gauge length and 3 mm in diameter. The universal tensile test machine (Autograph AGX 50 kN, Shidmazu) was applied for tensile test with strain rate and cross head speed of 5×10^{-4} s^{-1} and 6 mm/min, respectively.

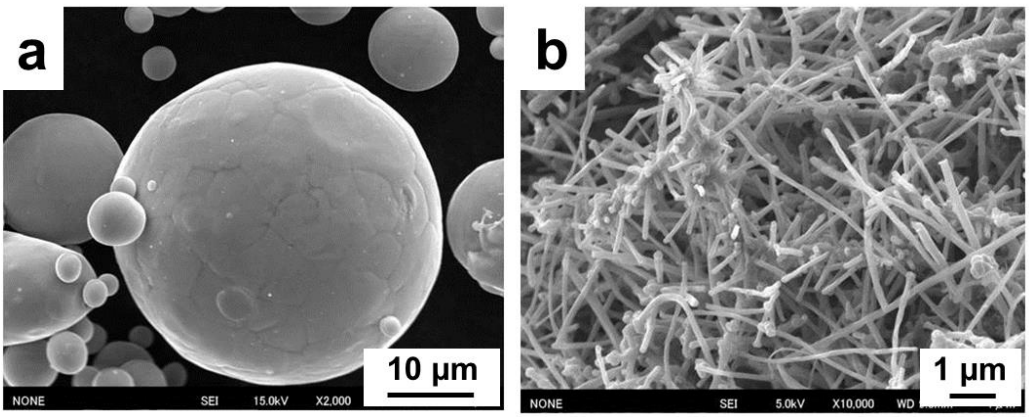

Fig. 1. SEM micrograph of (a) Ti-6Al-4V atomization raw powder, (b) Vapor grown carbon fibers (VGCFs).

Table 1. Chemical composition of Ti-6Al-4V atomization raw powder (wt-%).

Material	Al	V	Fe	C	O	N	H	Ti
Ti-6Al-4V	6.12	4.48	0.03	0.01	0.13	0.014	0.006	Bal

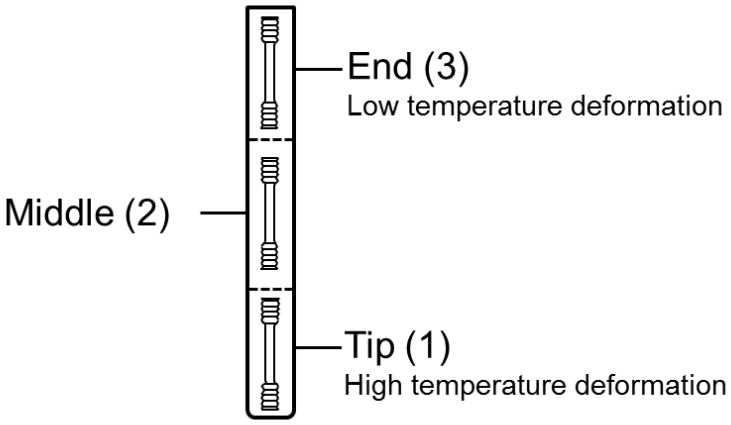

Fig. 2. Microstructure observation positions in extruded rod.

Results and discussion. The microstructures of Ti64 and Ti64+0.1wt-%VGCFs after SPSed including texture information such as pole figure (PF), inverse pole figure (IPF) and intensity of each plane direction are shown in fig.3. The monolithic Ti64 that was SPSed at 1273 K, which is above β transus temperature (1243 K) shows a large prior β grains of 170 μm (separated by yellow dash line) and α-lamellar colonies inside β grain (fig. 3a). The microstructure evolution was explained by the change of allotropy at 1243 K from α (hcp) to β (bcc) during heating followed by precipitation of α-lamellar phase inside grain and along the grain boundaries of prior β during cooling. On the other hand, Ti64+0.1wt-%VGCFs shows a different microstructure structures compared to monolithic Ti64 (fig. 3b). The microstructure of Ti64+0.1-wt%VGCFs consisted of α-lamellar and α-equiaxed which formed during cooling from β region to α+β region, and α+β region to α region, respectively [13, 14]. This microstructure evolution was also observed in Ti64+0.4-wt%VGCFs. The difference in microstructure between monolithic Ti64 and Ti64/VGCFs composite material was explained by an effect of α stabilizer of carbon that increased β transus temperature of composite material. Crystal orientation of Ti64 and Ti64+0.1wt-%VGCFs after SPSed was shown in fig. 3c and 3d, respectively. The random crystal orientation was observed in both materials including Ti64+0.4wt-%VGCFs, which was similar to cast alloy [15].

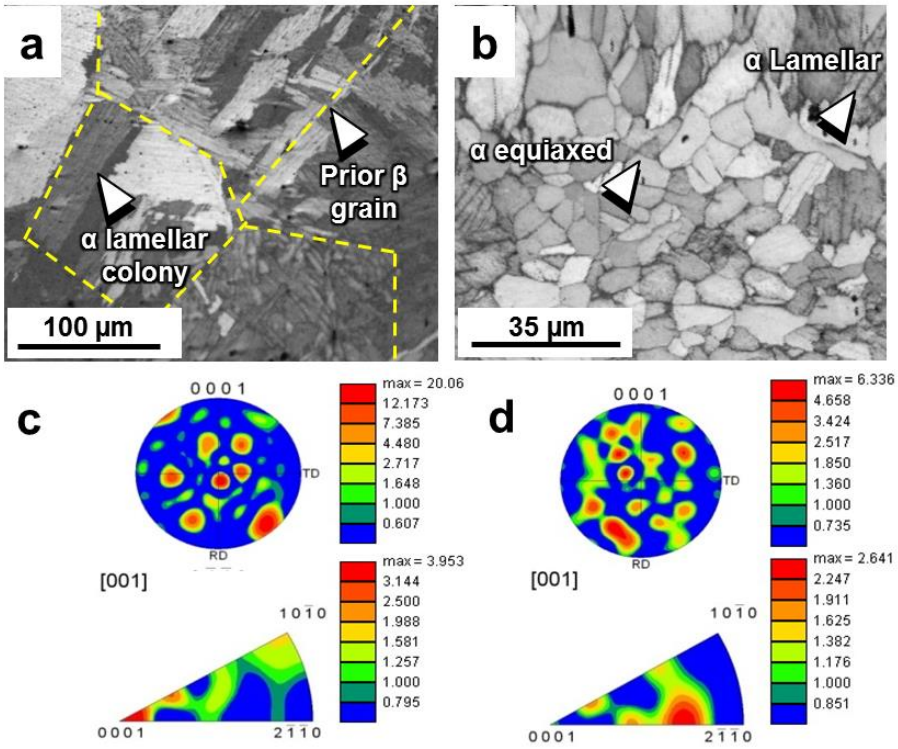

Fig. 3. SEM micrograph of (a) Ti64 and (b) Ti64+0.1wt-%VGCFs with attached pole figure (PF) and inverse pole figure (IPF) of (c) Ti64 and (d) Ti64+0.1wt-%VGCFs.

The microstructure of Ti64 and Ti64+0.4-wt%VGCFs observed from different positions in extruded rod in transversal direction by optical microscope were shown in fig. 4. Henceforth, monolithic Ti64, Ti+0.1-wt%VGCFs and Ti+0.4-wt%VGCFs will be name as T0, T0.1 and T0.4, respectively. Figure 4 shows a microstructure of T0-1 and T0.4-1 cut from a tip of extruded rod (A-X represents a sample name, in which A is a material and X is a position in extruded rod showed in fig. 2). A fine α-lamellar and α-equiaxed structure compared to SPSed sample was observed in extruded sample due to an effect of plastic deformation. The size of α-lamellar colony and α-equiaxed observed in T0 and T0.4 at position 2 and 3 (fig. 4b-4c and 4e-4f) was finer compared to sample obtained from position 1 (fig. 4a and 4d). This phenomenon was also observed in Ti0.1 as well. A large additional amount of VGCF in Ti0.4 resulted in a carbide phase formation, its periodic formulae was evaluated by EDS as $Ti_6C_{3.75}$.

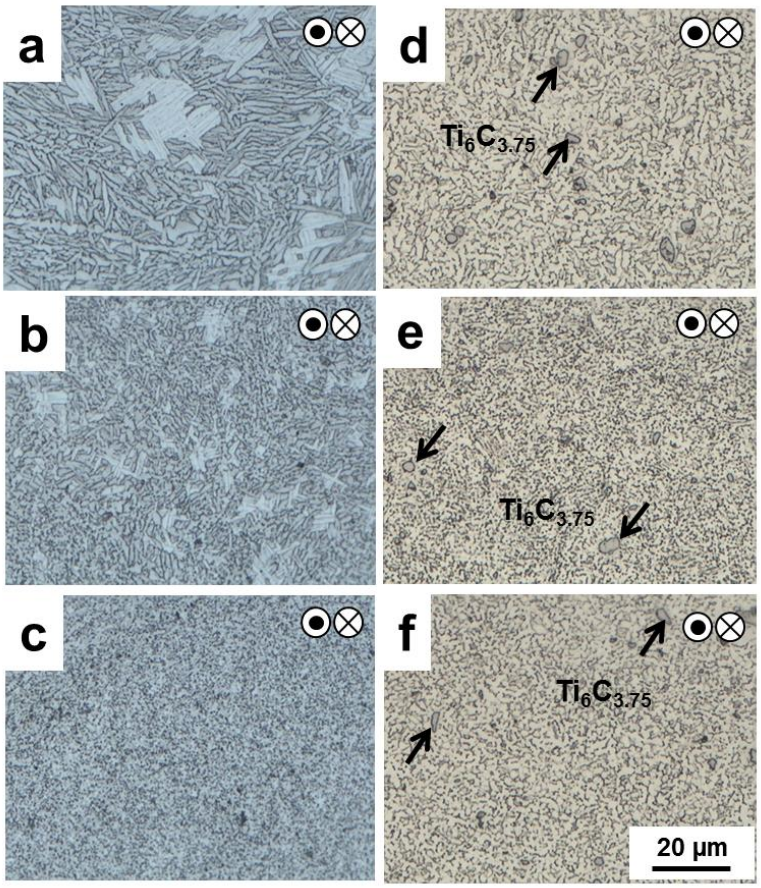

Fig. 4. Optical microstructure of Ti64 (a) T0-1; (b) T0-2; (c) T0-3 and Ti64+0.4-wt%VGCFs (d) Ti0.4-1; (e) Ti0.4-2; (f) Ti0.4-3 in transversal direction.

Figure 5 shows crystal orientation, pole figure (PF) and inverse pole figure (IPF) from three positions in Ti0 rod analyzed by EBSD. Figure 5a shows a crystal orientation of Ti0-1, which was extruded at temperature higher than β transus (1243 K). This sample exhibited a strong intensity in [0001] direction which parallel to extrusion direction, and a grain size of 16 μm was observed. Ti0-2, which was extruded at temperature lower than β transus (1173 K), shows some small nucleated grains on microstructure with a decreasing in intensity in [0001] direction. This sample shows a grain size of 10 μm, which was smaller, compared to Ti0-1 (fig. 5b). For Ti0-3, this position was extruded at temperature lower than 1173 K. A very small grain size of 1.3 μm and a large amount of nucleated grain was observed, grain morphology was changes from α-lamellar to α-equiaxed. The intensity in [0001] direction was decreased compared to Ti0-2. These results indicated that a dynamic recrystallization (DRX) was occurred in Ti0-3 sample (fig. 5c). The important factor that induced a DRX during hot extrusion was a deformation temperature, which different at each position in extruded rod. The deformation temperature will control a stored energy in extruded material [16]. Ti0-1 was extruded at highest temperature compared to other position (over β transus temperature), deformation at high temperature in a β phase region lead to an insufficient stored energy for DRX. The stored energy in Ti0-2 (fig. 4b) was higher than Ti0-1 because more defects such as dislocation and stress was generated in a material deformed at low temperature compared to high temperature [17]. Similarly, a large amount of dislocations was generated in a material after cold deformation. This phenomenon was clearly observed in Ti0-3, a high degree of DRX resulted in a random crystal orientation.

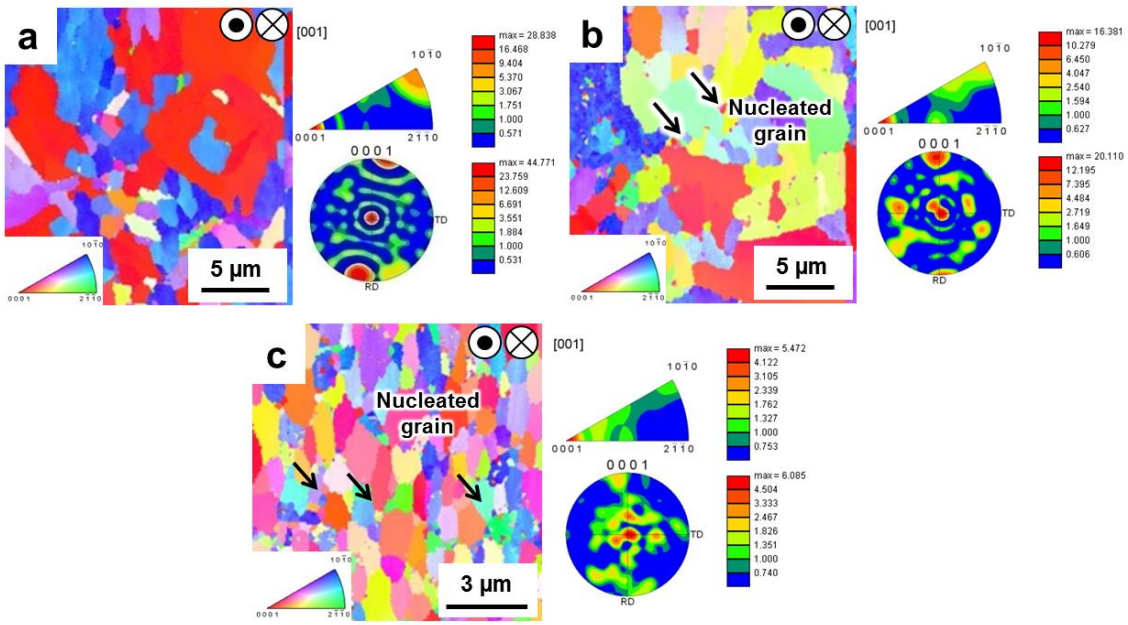

Fig. 5. Crystal orientation, inverse pole figure (IPF) and pole figure (PF) in transversal direction of (a) Ti0-1; (b) Ti0-2; (c) Ti0-3.

Figure 6 shows a crystal orientation, PF and IPF of extruded Ti composited with 0.1 wt-%VGCFs. Ti64 with 0.1wt-%VGCFs shows a nucleation of new grain in a high extruded temperature position (fig. 6a). The grain morphology of Ti0.1-1 was different from Ti0-1 because microstructure of Ti+0.1wt-%VGCFs was α-equiaxed after SPSed. An average grain size of Ti0.1-1 was 2 μm after extrusion but not uniform. The microstructure of Ti0.1-1 composed of prior α-equiaxed grain and a small nucleated grain, which indicated that DRX was not completed due to low stored energy. The small nucleated grain was ceased to growth during cooling, and a final microstructure was non-uniform. A DRX was easier to observe in samples mixed with VGCFs compared to monolithic Ti64 because an interstitial solid solution of carbon in Ti64 matrix acted as a defect, which increased a stored energy when material was deformed [16]. Ti0.1-2 shows a similar grain morphology, grain size and intensity in [0001] direction to Ti0.1-1 (fig. 6b). However, Ti0.1-3 shows a uniform grain size of 1.5 μm, and intensity in [0001] direction was decreased compared to Ti0.1-2 (fig. 6c). The uniform grain size and a random crystal orientation indicated that Ti0.1-3 exhibited higher DRX degree compared to Ti0.1-2 [18].

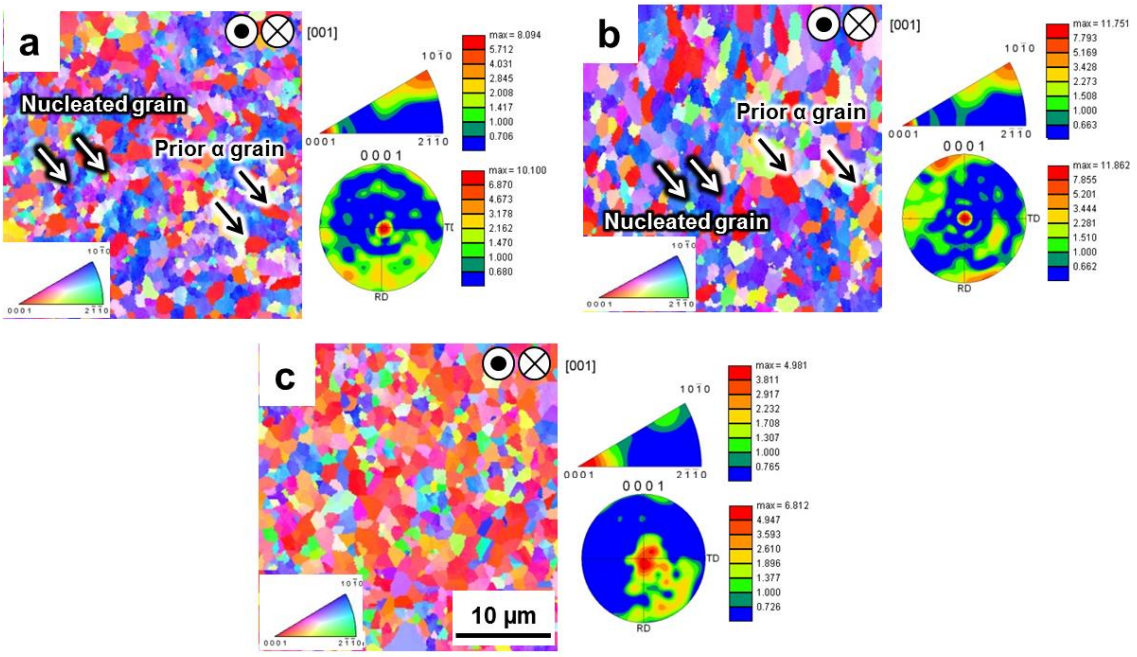

Fig. 6. Crystal orientation, inverse pole figure (IPF) and pole figure (PF) in transversal direction of (a) Ti0.1-1; (b) Ti0.1-2; (c) Ti0.1-3.

Figure 7 shows a crystal orientation, PF and IPF of extruded Ti composited with 0.4wt-%VGCFs. Ti64+0.4wt-%VGCF shows a similar microstructure to Ti64+0.1wt-%VGCF that a small nucleated grain and prior α-grain with a size of 2 μm was observed in Ti0.4-1 and Ti0.4-2 (fig. 7a and 7b). For Ti0.4-3, a uniform grain size of 1.5 μm was observed after nucleated grain growth, and a lowest intensity in [0001] direction among three samples was detected (fig. 7c). From crystal orientation, PF and IPF results, a DRX was strongly depended on a stored energy in a material. The stored energy was increased by decreasing of deformation temperature or an effect of solid solution of carbon. A. LUCCI et al. reported that an addition of various substitution alloying elements to Cu in a low content enable to induced a dynamic recrystallization after deformation by increasing a stored energy in a material [19].

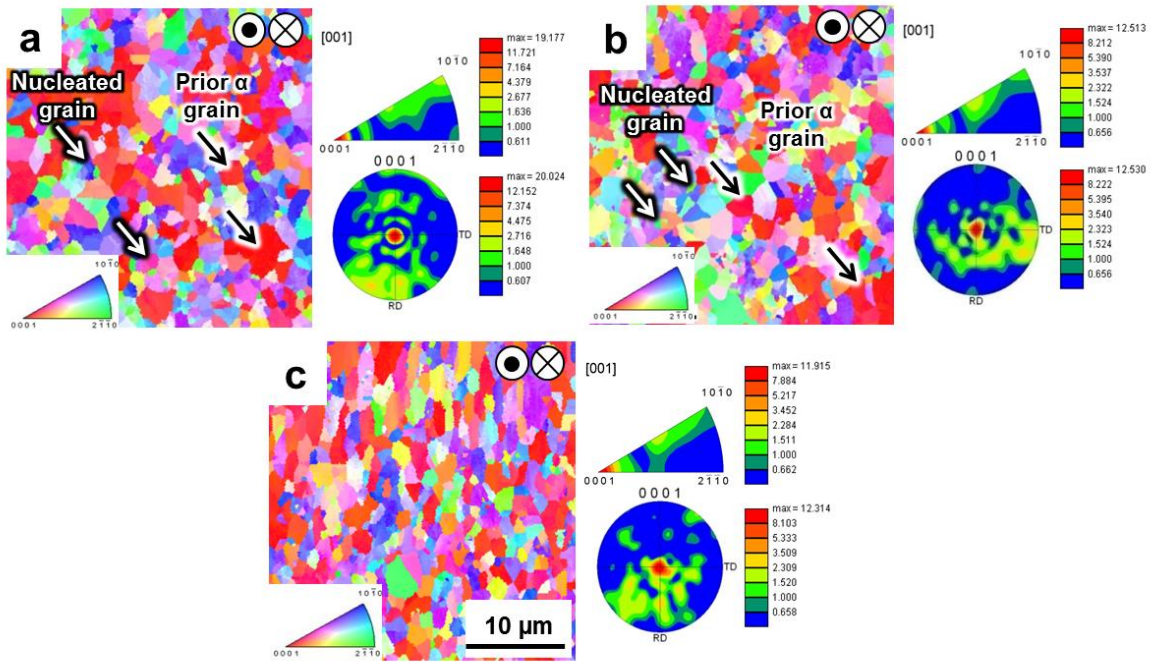

Fig. 7. Crystal orientation, inverse pole figure (IPF) and pole figure (PF) in transversal direction of (a) Ti0.4-1; (b) Ti0.4-2; (c) Ti0.4-3.

Tensile properties of Ti64, Ti64+0.1wt-%VGCF and Ti64+0.4-wt%VGCF obtained from different position in extruded rod were listed in table 2. For all materials, the lowest and highest of 0.2%YS and UTS was obtained from tip and end of extruded rod, respectively. During hot extrusion, position 1 was extruded at highest temperature (the first part to be extruded) compared to other position resulted in a low shear stress, and small amount of dislocation was formed in material. The flow stress was decreased by increasing of deformation temperature [3]. Samples that were obtained from position 2 and 3 show an increasing in tensile strength and yield strength compared to position 1 instead of decreasing because of dislocation removal by an effect of DRX. This was implied that shear stress generated by hot extrusion induced a DRX, and simultaneously generated a new dislocations at grain boundary during DRX. The size of new grains were very fine (fig. 4c and 4f) then a considerable amount of dislocations was formed in material resulted in an improvement of tensile strength with a traded off of elongation. Ti64 composite with VGCFs exhibited higher tensile strength compared to monolithic Ti64 obtained from same position because an effect of solid solution strengthening of carbon [20]. 0.2%YS and UTS of Ti64+0.4wt-%VGCFs was small decreased compared to Ti64+0.1wt-%VGCFs for sample obtained from same position due to a large amount of brittle carbide phase formation (fig. 4).

Table 2. Tensile properties of Ti0, Ti0.1 and Ti0.4 obtained from different position in extrusion rod.

Position	Ti64			Ti64+0.1wt-%VGCF			Ti64+0.4wt-%VGCF		
	UTS (MPa)	0.2%YS (MPa)	Elongation (%)	UTS (MPa)	0.2%YS (MPa)	Elongation (%)	UTS (MPa)	0.2%YS (MPa)	Elongation (%)
1	990	943	15.2	1127	1087.0	17.7	1191	1069	10.9
2	1121	1002	12.9	1166	1165	18.1	1150	1150	9.1
3	1131	1092	9.4	1190	1170	12.0	1192	1192	7.4

Stress-strain curve of Ti0, Ti0.1 and Ti0.4 extruded material obtained from different positions in extruded rod was shown in fig.8. For monolithic Ti64, Ti0-1 and Ti0-2 shows ductile behaviour that stress-strain curve exhibited no yield point. On the other hand, Ti0-3 obtained from DRX region exhibited a yield point in stress-strain curve with highest UTS of 1130.8 MPa (fig. 8a). This is because a considerable amount of dislocation formed in a part that extruded at low temperature. In the case of Ti0.1, yield point was observed in Ti0.1-2 and Ti0.1-3 (fig. 8b and c). From a principle, yield point was developed in a material that gained a sufficient shear stress, resulted in a permanent displacement of atom [9]. This was occurred in sample which experienced a deformation at low temperature such as the end part in extruded rod. For Ti64/VGCFs composite material, yield point was observed in samples obtained from position 2 because interstitial solid solution of carbon provided an additional shear stress in material [20]. Ductility of Ti0.4 was much lower than monolithic Ti0 and Ti0.1 due to a formation of large amount of $Ti_6C_{3.75}$ brittle intermetallic phase.

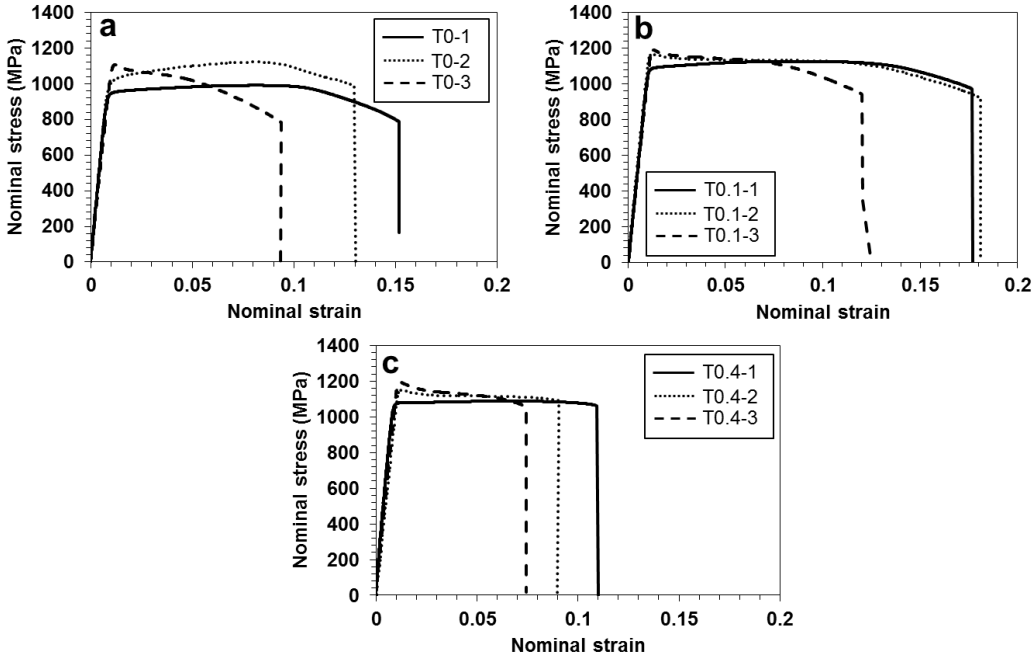

Fig. 8. Stress-strain curve of extruded materials obtained from different positions (a) Ti0; (b) Ti0.1; (c) Ti0.4.

Summary. The high stored energy in monolithic Ti or Ti composites was obtained when material experienced a deformation at low temperature or by an effect of solid solution of carbon, resulted in a DRX. The improvement of tensile strength of Ti0, Ti0.1 and Ti0.4 was obtained by DRX followed by dislocation formation during hot extrusion. The details are mentioned below.

1. The dynamic recrystallization (DRX) was occurred in sample that extruded at low temperature resulted in high stored energy in material. The small recrystallized grain was observed as evidence.

2. The solute carbon atom from vapor grown carbon fibers (VGCFs) in Ti64/VGCFs composite materials acted as a defect that provided additional stored energy in material during hot extrusion, and facilitate a DRXed.

3. The formation of dislocations at grain boundary during DRX at low deformation temperature which many small nucleated grains were formed resulted in improvement in yield and tensile strength. The increased value was small but systematically occurred for all samples.

References

[1] L.G. Zhen and L.R. Ze, Non-aerospace application of Ti materials with a great many social and economic benefits in China, Mater. Sci. Eng. A, 2000, 280, 25-29, DOI: 10.1016/S0921-5093(99)00651-6.

[2] D. Mareci, R. Cheraliu, D.M. Gordin and T. Gloriant, Comparative corrosion study of Ti-Ta alloys for dental applications, Acta Biomater., 2009, 5, 3625-3639, DOI: 10.1016/j.actbio.2009.05.037.

[3] A. Momeni and S.M. Abbasi, Effect of hot working on flow behaviour of Ti-6Al-4V alloy in single phase and two phase regions, Mater. Des., 2010, 31, 3599-3604, DOI: 10.1016/j.matdes.2010.01.060.

[4] T. Seshacharyulu, S.C. Medeiros, W.G. Frazier and Y.V.R.K. Prasad, Hot working of commercial Ti-6Al-4V with an equiaxed α-β microstructure: materials modeling considerations, Mater. Sci. Eng. A, 2000, 284, 184-194, DOI: 10.1016/S0921-5093(00)00741-3.

[5] R. Ding, Z.X. Guo and A. Wilson, Microstructural evolution of a Ti-6Al-4V alloy during thermomechanical processing, Mater. Sci. Eng. A, 2002, 327, 233-245, DOI: 10.1016/S0921-5093(01)01531-3.

[6] G.Z. Quan, G.C. Lua, J.T. Liang, D.S. Wu, A. Mao and Q. Liu, Modelling for the dynamic recrystallization evolution of Ti-6Al-4V alloy in two-phase temperature range and a wide strain rate range, Comput. Mater. Sci., 2015, 97, 136-147, DOI: 10.1016/j.commatsci.2014.10.009.

[7] H.Z. Niu, Y.F. Chen, Y.S. Zhang, J.W. Lu, W. Zhang and P.X. Zhang, Phase transformation and dynamic recrystallization behaviour of a β-solidifying γ-TiAl alloy and its wrought microstructure control, Mater. Des., 2016, 90, 196-203, DOI: 10.1016/j.matdes.2015.10.133.

[8] D.L. Ouyang, M.W. Fu and S.Q. Lu, Study on the dynamic recrystallization behaviour of Ti-alloy Ti-10V-2Fe-3V in β processing via experiment and simulation, Mater. Sci. Eng. A, 2014, 619, 26-34, DOI: 10.1016/j.msea.2014.09.067.

[9] H. Liang, H. Guo, Y. Ning, X. Peng, C. Qin, Z. Shi and Y. Nan, Dynamic recrystallization behaviour of Ti-5Al-5Mo-5V-1Cr-1Fe alloy, Mater. Des., 2014, 63, 798-804, DOI: 10.1016/j.matdes.2014.06.064.

[10] C.H. Park, J.H. Kim, J.T. Yeom, C.S. Oh, S.L. Semiatin and C.S. Lee, Formation of a submicrocrystalline structure in a two-phase titanium alloy without severe plastic deformation, Scr. Mater., 2013, 68, 996-999, DOI: 10.1016/j.scriptamat.2013.02.055.

[11] Y.Q. Ning, X. Luo, H.Q. Liang, H.Z. Guo, J.L. Zhang and K. Tan, Competition between dynamic recovery and recrystallization during hot deformation for TC18 titanium alloy, Mater. Sci. Eng. A, 2015, 635, 77-85, DOI: 10.1016/j.msea.2015.03.071.

[12] Y. Chen, J. Li, B. Tang, H. Kou, X. Xue and Y. Cui, Texture evolution and dynamic recrystallization in a beta titanium alloy during hot-rolling process, J Alloys Compd., 2015, 618, 146-152, DOI: 10.1016/j.jallcom.2014.08.129.

[13] G.C. Obasi, OM. Ferri, T. Ebel and R. Bormann, Influence of processing parameters on mechanical properties of Ti-6Al-4V alloy fabricated by MIM, Mater. Sci. Eng. A, 2010, 527, 3929-3935, DOI: 10.1016/j.msea.2010.02.070.

[14] G.G. Yapici, I. Karaman, Z.P. Luo and H. Rack, Microstructure and mechanical properties of severely deformed powder processed Ti-6Al-4V using equal channel angular extrusion, Scr. Mater., 2003, 49, 1021-1027, DOI: 10.1016/S1359-6462(03)00484-6.

[15] S. Roy, S. Suwas, S. Tamirisakandala, R. Srinivasan and D.B. Miracle, Microstructure and texture evolution during extrusion of boron modified Ti-6Al-4V alloy, Mater. Sci. Eng. A, 2012, 540, 152-163, DOI: 10.1016/j.msea.2012.01.120.

[16] J.D. Verhoeven, Fundamentals of Physical Metallurgy, 1st edn, 55-74; 1975, Canada, John Wiley and sons, Inc, ISBN: 978-0-471-90616-2.

[17] I. Sen, R.S. Kottada and U. Ramamurty, High temperature deformation processing maps for boron modified Ti-6Al-4V alloys, Mater. Sci. Eng. A, 2010, 527, 6157-6165, DOI: 10.1016/j.msea.2010.06.044.

[18] H. Matsumoto, M. Kitamura, Y Li, Y. Koizumi and A. Chiba, Hot forging characteristic of Ti-5Al-5V-5Mo-3Cr alloy with single metastable β microstructure, Mater. Sci. Eng. A, 2014, 611, 337-344, DOI: 10.1016/j.msea.2014.06.006.

[19] A. Lucci, G. Riontino, M.C. Tabasso, M. Tamanini and G. Venturello, Recrystallization and stored energy of dilute copper solid solutions with substitutional transition elements of the 4th period, Acta Metall., 1978, 26, 615-622, DOI: 10.1016/0001-6160(78)90113-X.

[20] F. Pedix, M.-F. Trichet, J.-L. Bonnentian, M. Cornet and J. Bigot, Relationships between interstitial content, microstructure and mechanical properties in fully lamellar Ti-48Al alloys, with special reference to carbon, Intermetallics, 2010, 9, 807-815, DOI: 10.1016/S0966-9795(01)00066-8.